Research Article

# Stress-induced degradation of 5 mol% yttria–zirconia in water at 300 °C

W. Vandermeulen[1] · R.-W. Bosch[1]



**Abstract**
5 mol% yttria–zirconia ceramic was studied for its use as solid electrolyte in high-temperature pH sensors since this material has interesting mechanical and ion-conducting properties and is available on an industrial scale. However, although its fracture mode in air is transgranular, some batches showed severe *intergranular* cracking in the working medium, water at 300 °C. In a previous study, it was found that the degradation could be related to the stress caused by the martensitic transformation of intergranular tetragonal precipitates. The aim of present study was to prove this assumption by experiment. To simulate the effect of transforming grain boundary precipitates, a nearly precipitate free material was subjected to an *externally* applied stress while exposed to 300 °C water. It was found that this also led to degradation by intergranular fracture. This proved the effect of tensile stress, but it also showed that the occurrence of *intergranular* fracture cannot be attributed solely to the location of the transforming precipitates at the grain boundaries. In an attempt to find the cause of the stress-induced intergranular fracture, 8 mol% yttria–zirconia was tested as well but this material showed only transgranular fracture. As a possible explanation, it is suggested that the occurrence of intergranular fracture in the 5 mol% yttria ceramic is not a property of the pure yttria–zirconia system but that sintering additives or impurities, segregated at the grain boundaries, could be the cause. However, examination of such segregation was not foreseen in the present study. Nevertheless, based on the present results it is thought that it should be possible to reduce degradation by a strict decrease of the amount and size of the intergranular tetragonal precipitates.

**Keywords** Yttria · Zirconia · 5 mol% · 8 mol% · Degradation · Water

## 1 Introduction

Zirconia ceramics are not only known for applications where mechanical strength, wear resistance and low thermal conductivity are required but also for applications based on ion-conducting properties, the so-called solid electrolytes [1, 2].

5 mol% $Y_2O_3$–$ZrO_2$ (5YSZ), used as the main material in the present study, is industrially produced and used as sensor electrolyte to measure the oxygen content in liquid steel [3]. For reasons of availability, strength and conductivity, it is also being evaluated for more advanced applications. As such it is studied for use in solid state oxygen pumps to control the oxygen level in molten eutectic lead–bismuth alloys, used as the coolant in advanced nuclear reactors [4, 5]. Another advanced application under consideration is as cladding protection material in supercritical water reactors [6].

On a somewhat shorter timescale, it was used as electrolyte for pH sensors in corrosion test installations, simulating nuclear power reactor conditions, i.e. water at 300 °C [7, 8]. However, during tests in hot water it was found that some batches showed intergranular cracking within 100 h while others remained intact for more than 1500 h. Therefore, a study was initiated to characterize the structural differences between "degradation sensitive" and

✉ W. Vandermeulen, wvanderm@sckcen.be; R.-W. Bosch, rbosch@sckcen.be | [1]Belgian Nuclear Research Centre, Boeretang 200, 2400 Mol, Belgium.

SN Applied Sciences (2019) 1:1034 | https://doi.org/10.1007/s42452-019-0967-5

Received: 4 March 2019 / Accepted: 22 July 2019 / Published online: 15 August 2019

"degradation resistant" batches. In this study, samples from different batches were exposed for different times in water at 300 °C in an autoclave. After exposure, they were examined for the presence of cracks. An extensive description of the obtained results was published previously but an overview of the most important observations will be given below [9]. However, because of the rather complex structure of the material a short description of the yttria–zirconia phase diagram will be given first [10].

Pure zirconia ($ZrO_2$) may have three different crystallographic structures: cubic above 2400 °C, monoclinic below 1200 °C and tetragonal in the intermediate temperature range. The transformation from tetragonal to monoclinic occurs by a martensitic mechanism. Due to the accompanying shape and volume change, cracks form and render the pure zirconia useless as a structural material. However, by adding 2–3 mol% yttria the tetragonal structure can be retained down to room temperature. The resulting material is strong, tough and wear resistant. Unfortunately, in the temperature range of 60–400 °C the presence of water or water vapour causes the martensitic transformation to occur [11–16]. Fragmentation of the material may happen rapidly unless the transformation is prevented by protecting layers or by using a grain size below about 0.5 µm [15, 17]. As will be seen later, this effect also contributes to the degradation of the 5YSZ sensor material.

Adding 8 mol% yttria (8YSZ) results in the stabilization of the cubic structure down to room temperature and avoids formation of the tetragonal phase. 8YSZ is a good oxygen ion conductor and is therefore used in solid oxide fuel cells and in electrochemical sensors [18]. It shows no degradation in hot water but its bending strength (300 MPa) was judged too low for its use in the pH sensor mentioned above [1, 16, 18, 19].

The material, subject of the present study, contains nominally 5 mol% yttria and 3–4 vol% alumina. Silica was definitely present, to a lesser extent, but was not determined quantitatively. Because knowledge of the structure is important for understanding the degradation behaviour, some data obtained in the previous study are reminded below [9]. Since the material is a commercial one, no information on the starting powders and sintering conditions is available.

The grains consist of a cubic matrix and have a size of the order of 40 µm. Two types of tetragonal precipitates are present. The so-called "large ones" are situated at the grain boundaries. In the batch with good degradation resistance, these particles have a diameter of around 3 µm and occupy about 3 vol%. In the degradation sensitive batches, these figures are, respectively, 11 µm and 8 vol%. Within the grains, a dispersion of small (50–200 nm) tetragonal precipitates is found. They are estimated to occupy roughly 50% of the volume. Such populations of sub-micron precipitates are well known to occur in zirconia ceramics [20–23]. A glassy phase, containing silicon and aluminium oxide, besides yttria and zirconia, was found but only at some grain boundaries and triple points. This may locally have caused intergranular fracture but globally its effect is thought to be negligible. Finally, alumina particles are present in the grains and at the grain boundaries. They behave rather inert since energy-dispersive spectroscopy (EDS) showed no presence of alumina in the zirconia phases and vice versa.

In a previous study, C-ring bending tests were performed at constant displacement rate of 0.5 mm/min in air at room temperature. The rupture stress was found to be between 400 and 600 MPa [9].

Constant load bending tests in air at room temperature always showed a transgranular fracture mode. Autoclave exposure caused spontaneous *intergranular* cracking. The amount of intergranular cracking was found to increase with the size and amount of the tetragonal grain boundary precipitates. From this observation, it was concluded that internal stresses, resulting from the water-induced martensitic transformation of the tetragonal grain boundary precipitates, were a prerequisite for degradation to occur.

The main aim of the present study was to demonstrate this conclusion. Therefore, the material with the lowest amount of intergranular precipitates, used in the previous study, was subjected to an *external* load in 300 °C water and examined for its degradation behaviour. The observations made are described in the following.

Finally, a limited attempt was made to compare the degradation behaviour of the 5YSZ with the behaviour of 8YSZ material under stress in water at 300 °C. This comparison was justified as follows. It was expected that, according to the phase diagram, the yttria content of the cubic 5YSZ grain matrix would be close to 8 mol%, and it might be expected that the degradation behaviour of the latter would be similar. This expectation turned out to be wrong as shown below.

## 2 Experimental and materials

The 5YSZ material is industrially produced as tubes with nominally 3 mm inner diameter and 6 mm outer diameter. Details on the composition and structure, obtained in a previous study, are given in the introduction. 8YSZ tubes were made on laboratory scale by isostatic pressing and sintering at 1500 °C of Tosoh TZ-8YS powder. The manufacturer data for this material mention (wt%), $Al_2O_3 < 0.1$, $SiO_2 < 0.02$, $Fe_2O_3 < 0.01$, $Na_2O < 0.12$. No glassy phase was observed at the grain boundaries.

The bending tests were conducted on C-ring specimens, cut with a diamond disc from one single tube to

avoid material variability. Outer and inner diameters of each specimen as well as the width were measured to 0.01 mm to calculate the stress. Different widths were used to obtain different bending stresses with a fixed applied force (Fig. 1a). The force was obtained by a single-piece deadweight resting on either three specimens or on one specimen and two dummies (Fig. 1b). The weight consisted of a steel cylinder with a mass of about 15 kg which fitted in the autoclave vessel without touching the walls. To calculate the stress, the buoyancy of the weight in the autoclave water was taken into account. Loading in air was done with the same weight as used in the autoclave.

The cylindrical surface of the specimens was left in the as-sintered condition. For the first tests, the flanks and edges were also left in the as-cut condition. For later tests, the specimen flanks were polished and the edges were chamfered to remove possible cutting defects which might affect crack initiation.

In the first tests, three specimens were mounted at 120° positions and carried each one third of the deadweight. The specimen supports, not shown in Fig. 1b, were designed to limit the drop of the loading weight upon rupture of a specimen. Yet, it could not be excluded that a minor shock, caused by rupture of one specimen, might cause fracture of another as well. Therefore, in subsequent tests only one sample was mounted and at the two other positions metal dummies were placed. Specimens which did not break during autoclave exposure were afterwards broken with pincers and examined for the presence of intergranular cracks which might have formed.

In order to examine the autoclave behaviour of the present material in the *absence of external* stress, samples with partially as-sintered and partially polished surfaces were exposed in the autoclave *without load* for times up to 1730 h. Both surface types were examined by optical (OM) and scanning electron microscopy (SEM). In addition, they were then broken in a bending test to provide a fracture surface for examination.

The water exposure was done at 300 °C in demineralized water containing 1000 ppm B and 2 ppm Li to stabilize the pH at 7.

SEM work was done with a JEOL JSM-6610 microscope, operated at 7 kV, using secondary electrons and spot size 40. Al sample surfaces were coated with platinum to avoid charging effects.

In one case, an intergranular fracture surface was etched in a 45/10/45 vol% mixture of $HNO_3/H_2O/HF$ to reveal the intragranular precipitates. Images of etched polished surfaces can be found in [8, 9].

## 3 Results on 5YSZ

### 3.1 Proof tests in air at room temperature

Specimens to be used in the autoclave were proof-tested under constant load in air at room temperature. About two thirds of the air-tested specimens survived proof tests at 200–250 MPa for around 50 h. Survivors were then tested in the autoclave.

The fact that a considerable number of ruptures occurred during proof testing shows that slow crack growth does occur in air at room temperature. Figure 2 shows an example of the crack initiation region in a specimen loaded under a stress of 350 MPa and which broke after 210 h. From the striation pattern, it follows that the crack origin is situated in the upper right corner where two crack orientation systems can be distinguished. It is thought that the cracks, indicated by "c", which are perpendicular to the applied stress, are caused by cutting of the specimen from the tube. These cracks are supposed to have grown slowly until at some place the critical stress intensity was reached, thus causing

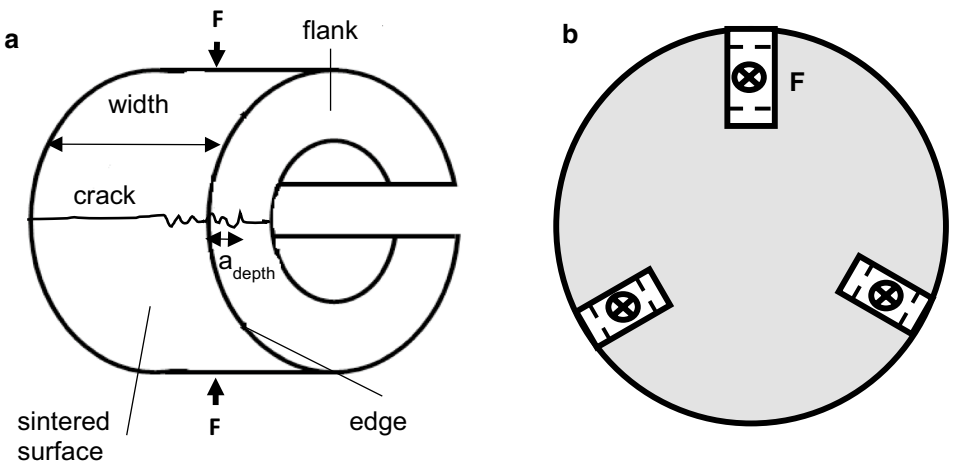


**Fig. 1** Specimen used for bending tests and loading system in the autoclave. **a** specimen shape; **b** positioning of specimens in autoclave, seen from above. The cylindrical deadweight (grey) rests equally on the three positions marked by a cross

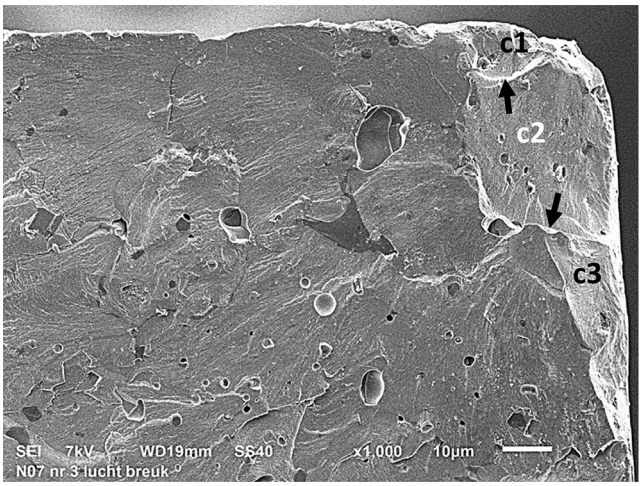


**Fig. 2** Fracture origin of specimen ruptured under 350 MPa in air at room temperature. Cracks c1, c2 and c3 are due to cutting; arrows indicate cracks perpendicular to the fracture surface, formed by joining of the c-cracks

complete fracture of the specimen. Other cracks which are more or less perpendicular to the fracture surface (indicated by arrows) are supposed to have formed to join the c-cracks. All cracks are transgranular.

On the main fracture surface no mirror, generally considered to indicate the region of slow crack growth, could be detected [24]. Supposing the critical stress intensity factor to be 2–4 MPa $m^{0.5}$, the critical crack size, supposed to be equal to a potential halo size, can be calculated from

$$KI = C\,6M\,(\pi a)^{0.5}/b^2$$

where $M$ is the bending moment, $a$ is the crack depth and $b$ is the wall thickness. $a/b$ was supposed to be 0.1 which makes $C$ near to one [25]. A halo size of roughly 30–100 µm was calculated for a bending stress of 350 MPa. The mirror should be clearly visible, if present, on the main fracture surface. Therefore, it has to be supposed that the transition from slow to fast crack growth occurs at some point along the complex set of cutting-induced defects and that no slow crack growth occurs along the main fracture surface.

All specimens which ruptured in air showed a similar fracture origin as shown in Fig. 2. It is therefore likely that most fractures in air are linked to machining defects as they start from the cut surface. For this reason, most autoclave specimens were chamfered or rounded at the edges.

## 3.2 Autoclave exposure without external stress

### 3.2.1 Examination of the as-sintered surface

Figure 3a shows an OM picture of the unexposed as-sintered surface. Shallow grooves, about 5 µm wide, mark the grain boundaries. Alumina crystals and tetragonal zirconia inclusions are visible. Figure 3b shows the as-sintered surface of a specimen, exposed for 523 h. The alumina crystals have been completely dissolved, and the crystal-like features are in fact polyhedral pits as could be seen by adjusting the microscope focus.

Nevertheless, it is clear that possible intergranular cracks cannot be detected by bright field observation in the OM. A more appropriate method, not further discussed here, has been published elsewhere [8].

SEM pictures of sintered surfaces in the as-received state and after unloaded autoclave exposure for 523 h

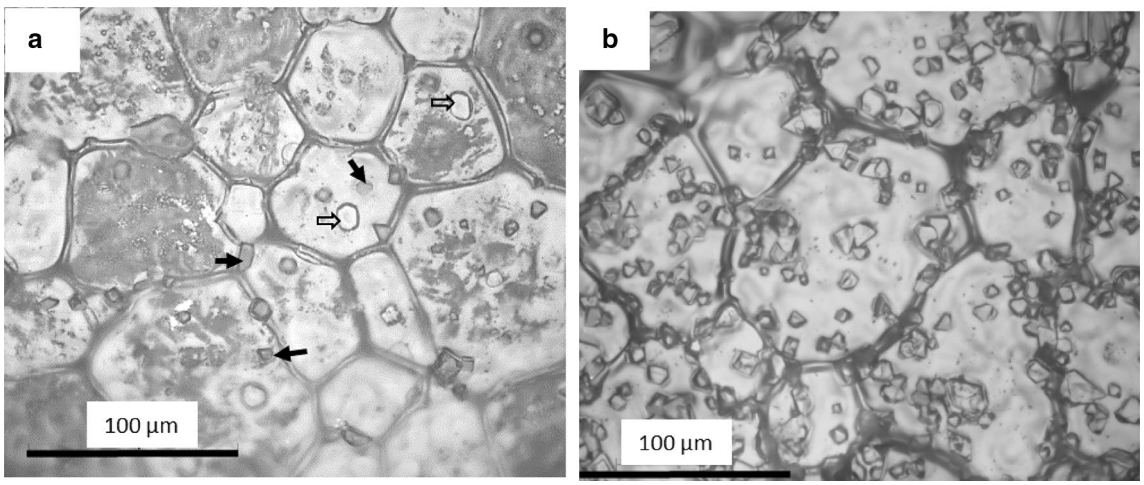


**Fig. 3** OM bright field pictures of as-sintered surface. Note shallow grooves along grain boundaries **a** as-received. Black arrows: alumina precipitates, white arrows: tetragonal precipitates, **b** after 523 h autoclave exposure. No cracks are visible. Crystal-like features are pits resulting from dissolution of alumina

are shown in Fig. 4a, c, respectively, 4b, d. In both cases, the grain boundary appearance is identical. It consists of the shallow depression along the grain boundaries, mentioned before. By SEM however, it can be seen that *in* this depression a narrow groove runs which is supposed to follow the actual grain boundary. These grooves are thought to result from thermal etching during sintering. They look similar on a non-exposed surface and on an exposed surface. This makes it difficult to distinguish a groove (of unknown but limited depth) from a groove with a subsurface crack. Precipitates can be seen at the grain boundaries. These are most likely tetragonal particles because they transform martensitically as can be deduced from the surface relief. Again, the distinction of grooves and cracks at the interface of these tetragonal particles is difficult to make with certainty.

### 3.2.2 Cracking observations on polished surfaces

On the polished areas which were exposed without load in the autoclave, cracks and the tetragonal precipitates are clearly visible in the optical microscope because of the surface relief caused by the martensitic transformation (Fig. 5). Cracks initiate at the interface between transformed tetragonal grain boundary precipitates. They are supposed subsequently to propagate along the grain boundaries under the stress field of the transformed particle. It may be mentioned here that a priori there is no reason for the cracks *not to propagate transgranularly*. This will be discussed later. The figure also shows that although cracking is frequent, the crack density is not sufficient to form a continuous network which would involve full fracture.

### 3.2.3 Observations on fracture surfaces

Several specimens were broken intentionally in air at room temperature after exposure in the autoclave without applied load. The fracture surfaces were examined by SEM. All fractures were found to start from a region with mixed intergranular and transgranular cracks connected to the surface, i.e. in contact with water (Fig. 6). Such fracture origins will be described in more detail in the following section on loaded specimens. The depth

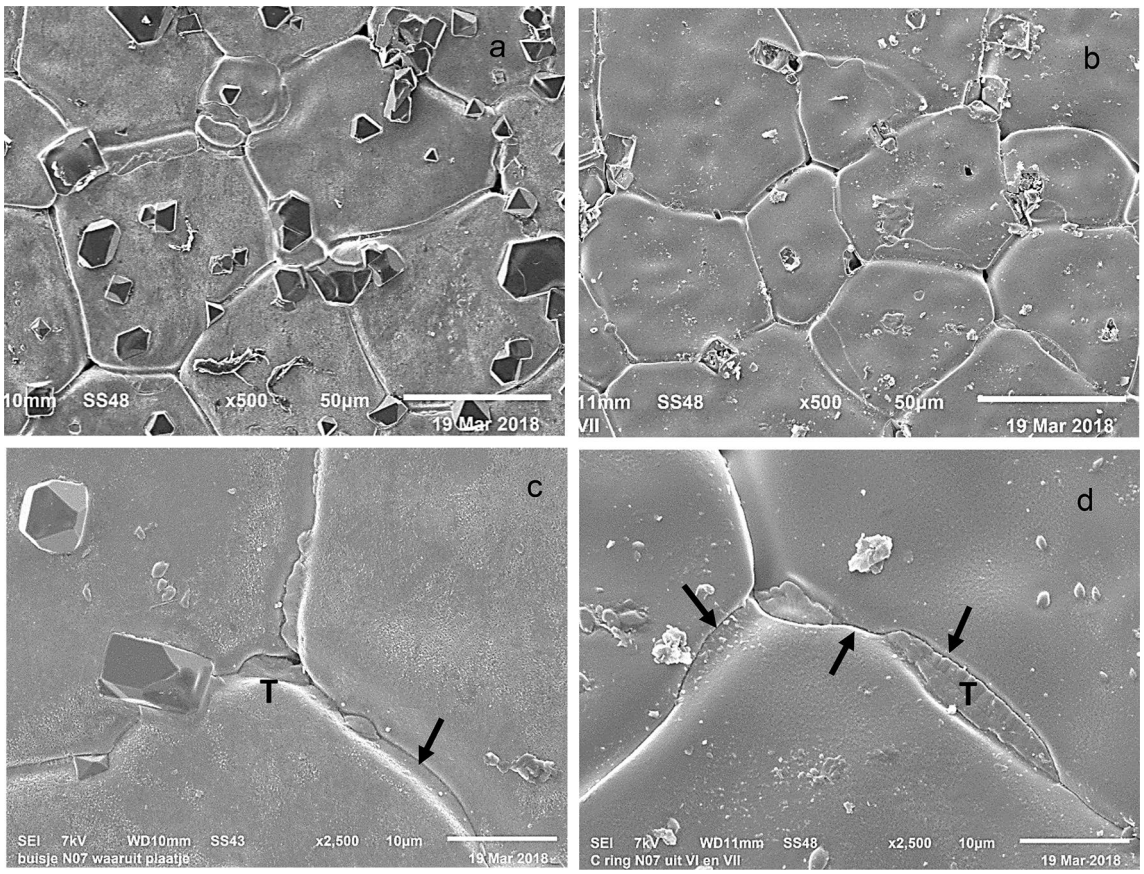


**Fig. 4** **a**, **c** As-sintered surface aspect without autoclave exposure; **b**, **d** after exposure. Dissolution of the alumina crystals is the only clearly visible effect. Sharp grooves along grain boundaries are indicated by arrows. T: tetragonal precipitates at grain boundary. Dark crystals are alumina

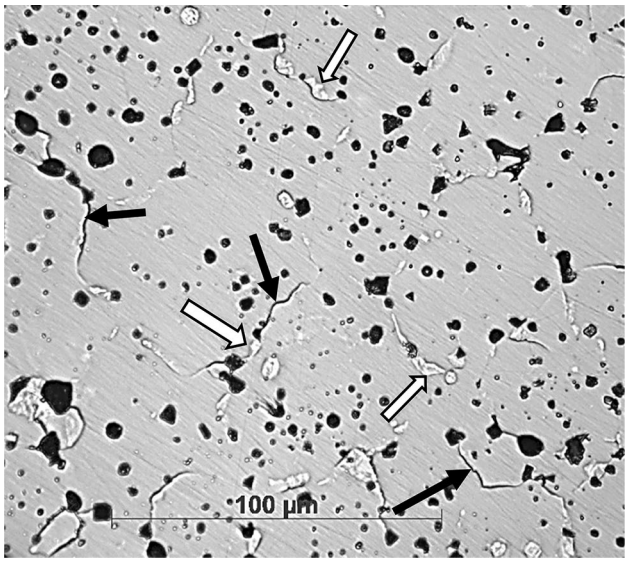


**Fig. 5** Polished surface, exposed unloaded for 523 h. White arrows: transformed tetragonal precipitates; black arrows: grain boundary cracks

of the area with mixed fracture, defined as its largest extent below the sintered surface, was measured and plotted versus the exposure time in Fig. 7. It was found that the depth of these regions was limited to about 100 µm, which corresponds to only two grain diameters, and that it shows no dependence on the exposure time. This suggests that this region develops fast but then stops growing, apparently due to lack of driving force. This driving force is expected to be insufficient because of the low content of tetragonal grain boundary precipitates [9].

## 3.3 Autoclave exposure on externally loaded samples

### 3.3.1 Stress versus rupture time results

Figure 8 shows a plot of the stress versus exposure time, i.e. the time a specimen spent in the autoclave. Closed circles represent specimens which did break during exposure. Open circles represent specimens which did not break during exposure. Some of the specimens which were not broken after a first run were loaded again for further exposure. It should be realized that the exposure time gives only an upper limit to the rupture time since no rupture detection system was available. By combining the lowest "broken" times with the highest "not-broken" times, an estimation of the real rupture time for different stresses was made as indicated by the trend lines in Fig. 8. Extrapolation to short times shows that very fast rupture can be expected for stresses above 200 MPa. Constant load testing in water at 300 °C thus reduces the bending strength obtained from constant rate tests at room temperature by roughly a factor of two. The fact that one specimen, tested at only 85 MPa did survive suggests that this stress is insufficient to cause rupture, thus pointing at the possibility of a lower threshold stress.

### 3.3.2 SEM examination of the fracture surfaces

The fracture surface of all specimens, either broken during or after exposure, was examined by SEM. It was found that most cracks started as a mixed mode zone similar to the unloaded samples discussed in Sect. 3.2. However, the size of these zones varied largely. Figure 9 shows three typical cases of mixed mode crack size, all broken in the autoclave under a stress of 200 MPa. Outside these zones, cracking is transgranular. The majority of the mixed mode fracture

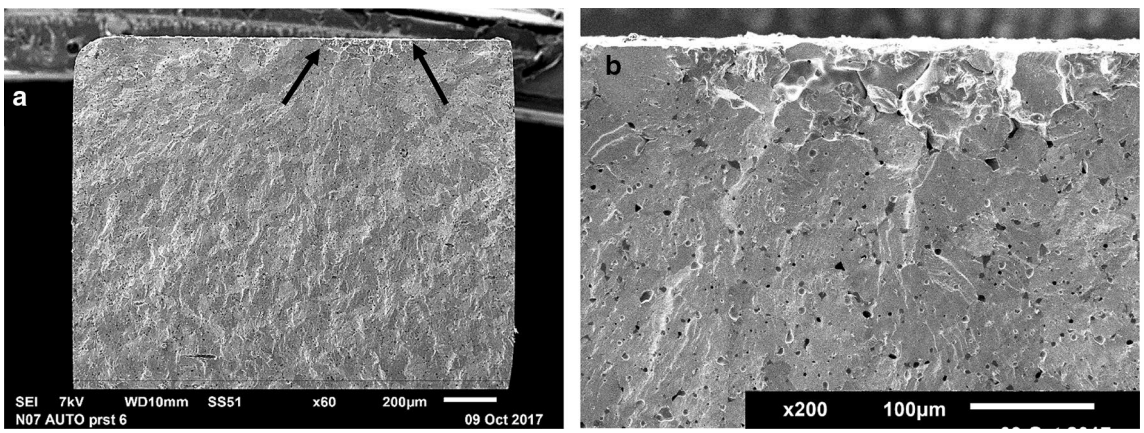


**Fig. 6** Specimen broken after 100 h unloaded autoclave exposure. **a** between arrow tips: fracture origin, **b** detail of previous showing mixed rupture mode near sintered surface

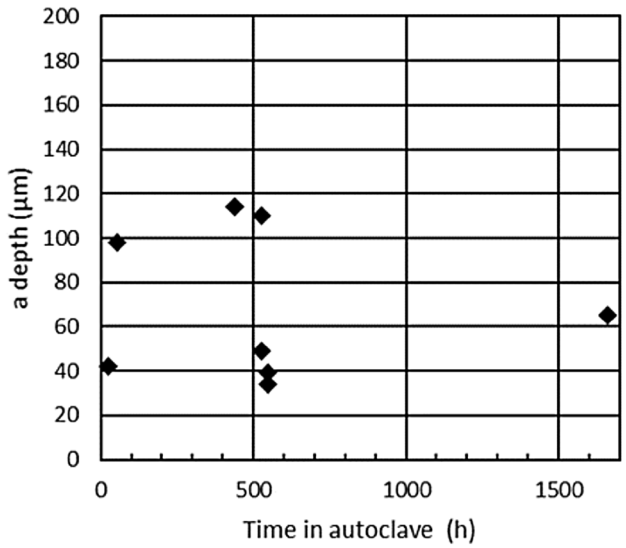


**Fig. 7** Size of the mixed mode fracture zone plotted versus unloaded exposure time. The specimens were broken after exposure

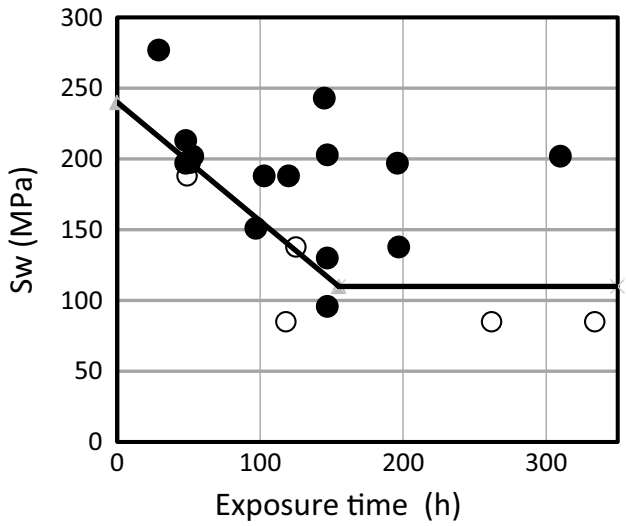


**Fig. 8** Stress (Sw) versus time in autoclave. Closed symbols: specimen broken during exposure; open symbols: specimen not broken after exposure. The straight lines give an estimation for the border between broken and not-broken specimens

zones are situated at a corner of the fracture surface, even if this was rounded or chamfered to remove machining cracks as discussed in Sect. 3.1. This indicates that crack initiation occurs preferentially at the flanks and rarely at the as-sintered surface. Possible reasons for this behaviour may be a difference in composition between the sintered and the cut surface or the effect of cutting itself.

The size of the mixed fracture zones was characterized by $a_{depth}$ since it was expected that this value was most characteristic for determining a stress intensity factor. Three size-groups can be distinguished.

(a) The small ones with depths up to 100 µm. These are in size similar to the cracks found in the specimens exposed without load. Therefore, they are expected to show only a limited contribution of the applied stress.
(b) Crack depths between 100 and 350 µm. These are expected to be caused by the stress applied during exposure.
(c) Very large cracks, with a depth of more than 400 µm. These suggest an unlikely high fracture toughness as will be discussed below.

### 3.3.3 Fracture toughness

From the river pattern in the transgranular fracture region, it can be seen that the mixed fracture region acts to start the purely transgranular crack which causes final rupture (Fig. 9). It is therefore likely that at the border between the two zones the critical stress state is reached which allows fast fracture, unaffected by the environment. $KI_c$ values were calculated for a geometry corresponding to an edge crack in a plate of given width, subjected to a crack opening bending moment *in the plane* of the plate [25]. The measured $a_{depth}$ was used as crack size, and the bending moment was calculated from the specimen dimensions and applied load (Fig. 1).

Figure 10 shows the calculated stress intensity factors in the testing order. The two white bars are data for specimens which formed a crack but did not break *during* exposure. The calculated KI for these two is therefore less than the critical one. The two other specimens with low $KI_c$ value (grey bars) are thought to have been broken accidentally during the test.

Six specimens broke at KI values between 3 and 5 MPa $m^{0.5}$. These can be considered as "normal" for the 5YSZ material. Four results are between 5 and 10 MPa $m^{0.5}$ which is unusually high. They were tested at about the same applied stress as the others, yet they show the four largest crack depths. A possible explanation for these results follows below.

### 3.3.4 Examination of the fracture mode

In the previous study, it was found that the mixed fracture mode resulted from a fully *three-dimensional* network of intergranular cracks [9]. Transgranular cracks were supposed to be caused in interlocking grains, bridging the crack upon failure. However, since it was found that slow transgranular cracking occurs in air at room temperature, as shown in Sect. 3.2, the possibility was envisaged

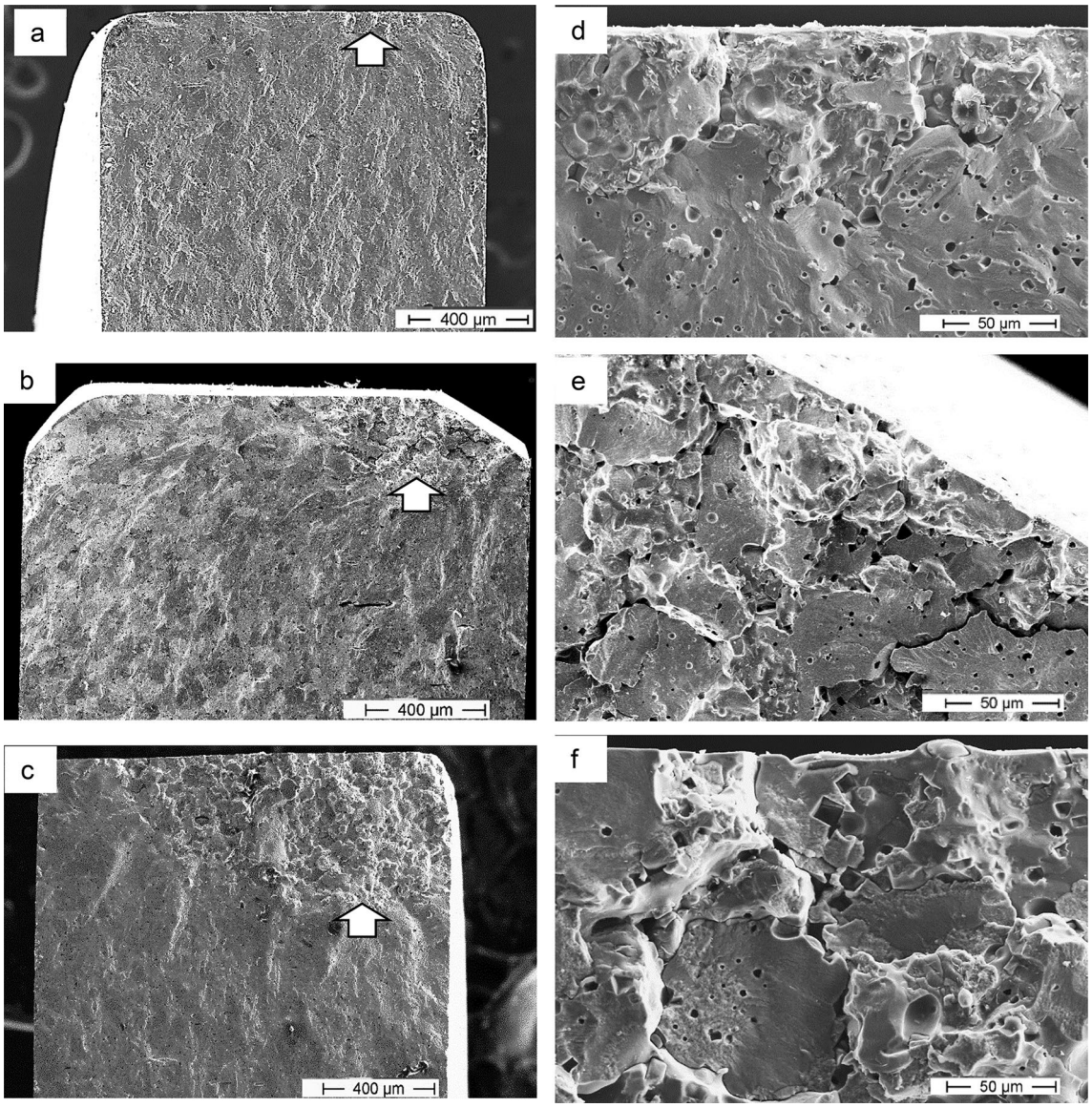


**Fig. 9** Fracture surfaces of specimens loaded at 200 MPa and exposed for, respectively, 75 h (**a**, **d**), 270 h (**b**, **e**) and 476 h (**c**, **f**). Note the difference of mixed mode crack depth (white arrows), although the same load has been applied

that cracking in the mixed fracture zone occurs by both inter- *and* transgranular slow crack growth. Therefore, additional observations were made to examine the three-dimensional extent of the cracks under external stress conditions and to look for indications of slow transgranular crack growth.

Figure 11 shows a cross section perpendicular to the crack plane of a specimen loaded for 147 h at 203 MPa, yielding a mixed mode crack depth of 470 µm. On this section, the fracture surface is generally intergranular except for the grain indicated by the white arrow pointing down. Below the fracture surface, only two short intergranular cracks, indicated by black arrows, can be seen. The idea of the formation of a *network* of intergranular cracks in the external tensile stress field is therefore not confirmed. It rather appears that one single two-dimensional *intergranular* crack propagates until fast rupture occurs.

This is supported by a closer examination of the fracture surface showing that many of the grains which broke transgranularly are surrounded by an intergranular crack. Figure 12 shows corresponding fracture areas on two specimen halves. Grains which broke transgranularly generally lie in a depression on one half and protrude on the other. It can be seen that only on the specimen half on which the grain lies in a depression, it is surrounded by an intergranular crack (Fig. 12a, b). This crack must have passed behind the grain and thus have been formed *before* the transgranular crack occurred. This shows that a fully intergranular

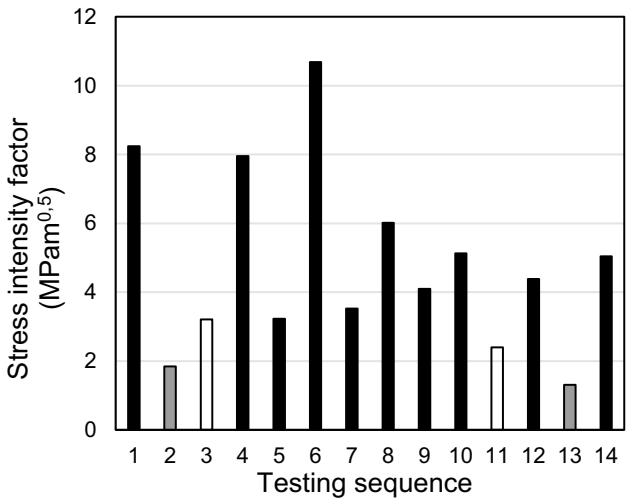


**Fig. 10** Loaded autoclave exposure tests. Stress intensity factor calculated from the size of the mixed fracture zone. Black: ruptured during exposure; white: broken intentionally after test; grey: probably accidental rupture

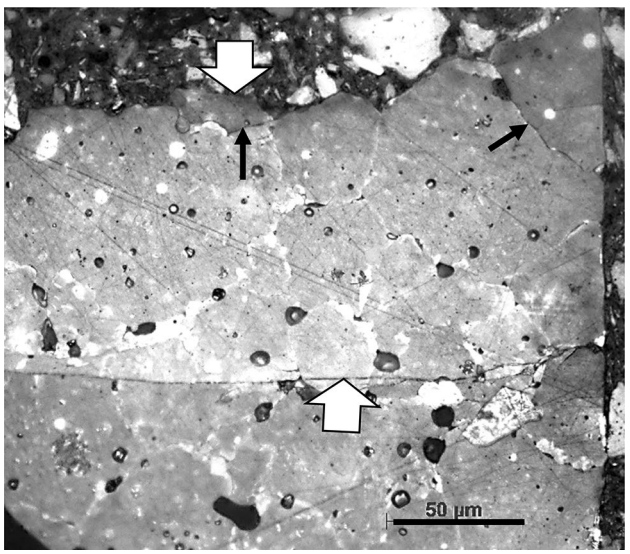


**Fig. 11** Cross section of specimen with intergranular fracture. Top: fracture surface; right: sintered surface. Black arrows show intergranular subsurface cracks. White arrow pointing down: grain which broke transgranularly. White arrow pointing up: transgranular crack caused by specimen mounting

crack forms first by meandering between the grains. Some of these grains rupture only afterwards transgranularly as explained in Fig. 12c, d. Therefore, these grains, by an interlocking or bridging mechanism, are expected to reduce the effective stress acting on the growing intergranular crack. This explains the occurrence of the very large mixed mode crack areas discussed in Sect. 3.3.2 which in turn yield the abnormally high $KI_c$ values.

The possible magnitude of the interlocking and bridging effect was estimated from room temperature constant rate bending tests on specimens in which an intergranular network was known to be fully developed three dimensionally by unloaded exposure. These specimens were obtained from tubes with high tetragonal phase content which were actually used as sensor. Although nearly all the grain boundaries were cracked, these specimens remained intact notwithstanding handling and cutting. C-ring bend tests showed rupture stresses between 100 and 230 MPa which is close to the stress applied in the present tests.

As for all the fracture surfaces observed till now, no indication of slow transgranular growth could be found in the mixed mode region, and neither could a difference be found between the transgranular crack appearance in the mixed mode zone and in the fully transgranular zone. It is therefore thought that the contribution to the fracture process of transgranular slow crack growth, if occurring, is of secondary importance.

Finally, a more detailed SEM examination of the intergranular fracture surface was made to compare it with the 8YSZ. Figure 13a shows that smooth regions are the most common and therefore must result from the grain boundaries between the cubic grains. Rougher areas result from the grain boundary precipitates. It is clear that the tetragonal sub-micron *intragranular* precipitates, which fill about 50% of the cubic grain interior, do not extend to the grain boundary. This means that the boundaries of the grains consist of a very thin cubic zone. According to the phase diagram, the yttria content of this zone should be close to 8 mol%. After etching for 30 min, this layer was found to be removed because the intra-grain tetragonal precipitates have become visible (Fig. 13b–d). It thus might be expected that both materials, 5YSZ and 8YSZ, would show the same grain boundary behaviour when loaded in hot water.

## 4 Results on 8YSZ

The 8YSZ material is single phase cubic with a grain size of around 3 µm. To examine the fracture mode, C-ring specimens of 8YSZ were tested in the same way as the 5YSZ.

Figure 14a shows the fracture surface of a specimen broken during a proof test in air. Fracture can be seen to have started from the defect in the upper left corner. Figure 14b shows a fracture which occurred under load in the autoclave, possibly starting from a pre-existing crack in the chamfered region. The specimen shown in Fig. 14c was exposed under load in the autoclave for 310 h under a stress of 102 MPa without rupture. It was broken after unloading.

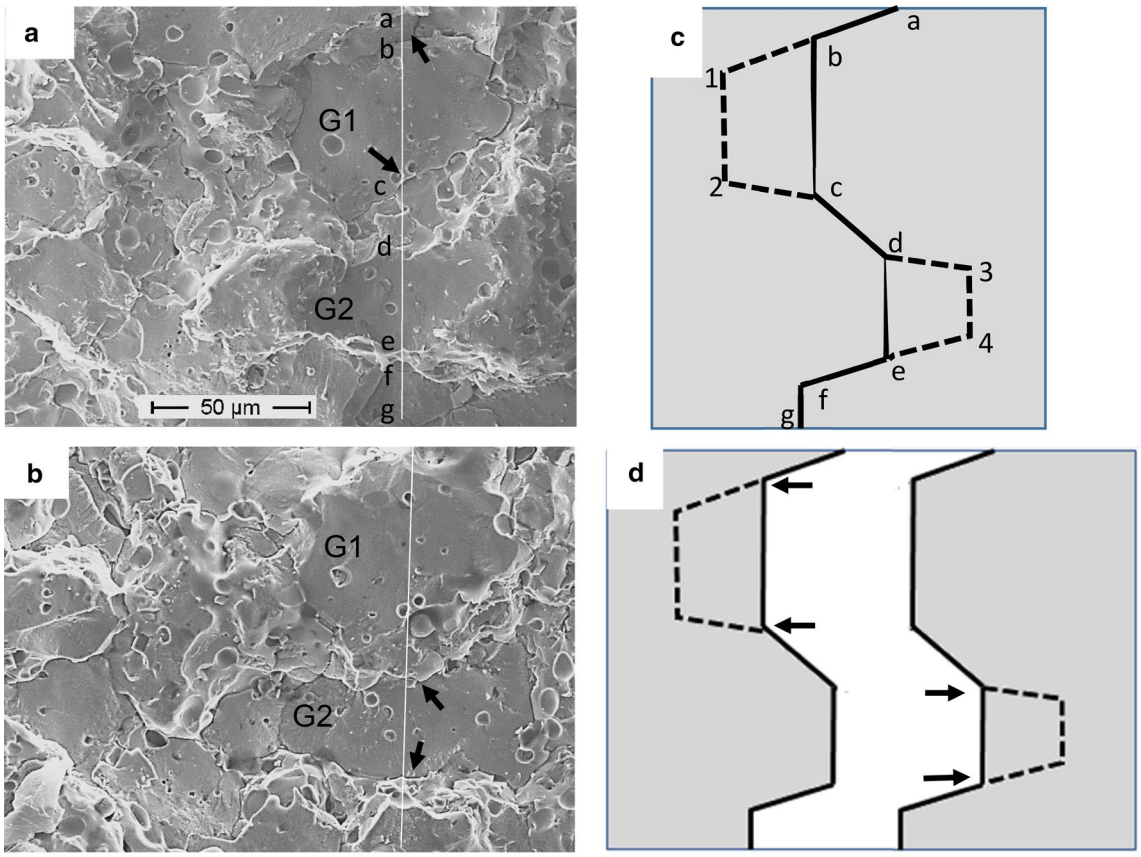


**Fig. 12** Corresponding fracture areas **a** grain G1: transgranular crack lying in a depression and surrounded by an intergranular crack; grain G2: transgranular crack protruding and not surrounded by an intergranular crack. **b** The opposite remarks apply for the other specimen half, **c** schematic cross section along line ag in figure a. The initial crack is intergranular and marked ab12cd34efg. **d** On separation of the two specimen halves grains, G1 and G2 broke transgranularly along planes *bc* and *de* which are surrounded by the intergranular cracks indicated by arrows. Note that one picture has been mirrored to ease comparison

These tests show *only transgranular* crack growth to occur in air at room temperature and in 300 °C water. Moreover, as far as could be seen from the limited number of tests and the uncertainty of the rupture time in the autoclave, no effect of the water environment on the rupture time of 8YSZ was found. The expectation that 8YSZ would behave similarly to 5YSZ clearly was not confirmed. This is further discussed below.

## 5 Discussion

Since most of the more detailed observations have been considered in the results section, this discussion will be limited to the major points raised during this study. Unless specified otherwise, observations and conclusions are supposed to be bear on the material selected for this study, i.e. 5YSZ *with low content of tetragonal precipitates.*

The autoclave tests on the *unloaded* specimens confirm that in this material, as expected from previous work, degradation does not occur or at least is strongly reduced. This is explained by the fact that only low internal transformation stresses are generated [9].

Tests under load show that application of externally applied stress, of the order of 200 MPa, causes *intergranular* crack growth in a plane approximately perpendicular to the stress. This clearly shows that the assumption that the presence of a stress is a prerequisite for degradation in 300 °C water is confirmed. This confirmation was the main incentive for this study. It also shows that the origin of the stress, external source or transformed precipitates does not matter.

Some additional points are worth mentioning. All autoclave specimens show that the intergranular fracture does not extend over the complete surface. It always consists of two regions: an initiation region, containing an intergranular (or mixed) fracture mode, followed by a final fracture region with purely transgranular fracture. This transition can be understood from the fact that the test is executed under constant load. At the start of the test, the critical

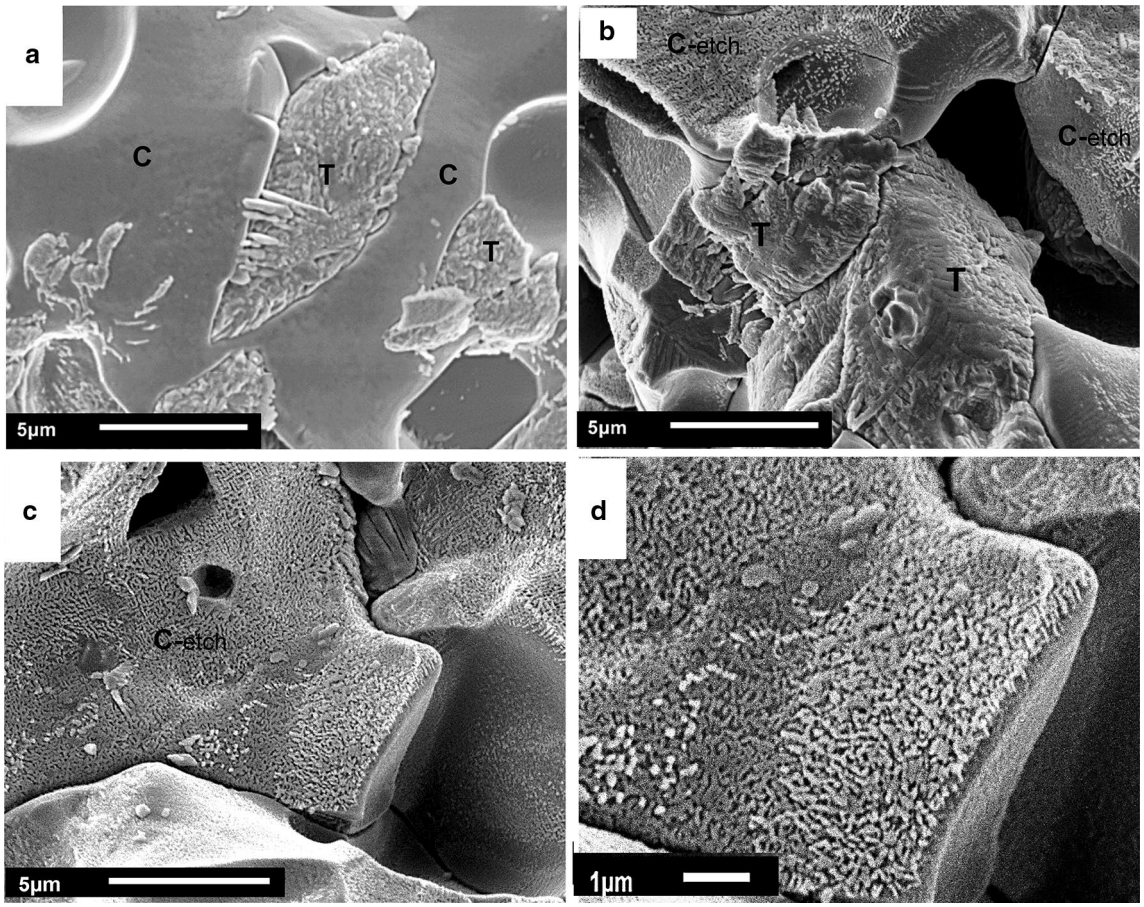


**Fig. 13** Intergranular fracture of sensor tube used in 300 °C water: **a** as fractured after service C: smooth areas, cubic–cubic grain boundary T: rough areas, tetragonal particle, **b** similar surface after etching C-etch: cubic–cubic grain boundary T: relative large tetragonal particles, **c** cubic grain boundary with population of intragranular tetragonal precipitates and **d** detail of previous

stress intensity factor for transgranular cracking is obviously not reached at any point. Therefore, *fast* transgranular cracking cannot occur and *slow* transgranular growth is negligible, as suggested by the tests at room temperature. Therefore, an intergranular crack can grow until the critical stress intensity for transgranular fracture is reached at its front and fast rupture takes place. Support for this model is found in the fact that acceptable $KI_c$ values could be calculated from the size of the intergranular region.

Another problem remains: why is intergranular cracking only found in water and not in air? The present results show that the fact that cracking is intergranular cannot be explained by the transformation stress of the tetragonal grain boundary precipitates. This assumption can be excluded because in the present material there are not sufficient precipitates as shown by the unloaded autoclave tests, yet intergranular cracking occurs when a load is applied. The small amount of precipitates may have contributed but is clearly not the primary cause. Moreover, it should be recognized that, except in special cases where the precipitates would cause systematically a tensile stress perpendicular to the grain boundaries, a randomly oriented stress source at a grain boundary might as well cause transgranular cracking as intergranular cracking.

An obvious conclusion would be to attribute the occurrence of intergranular fracture to the presence of water. Water is known to induce the martensitic transformation of the *tetragonal* phase. However, in the present case the intergranular cracking occurs along *cubic* grain boundaries, a phase which is known to be stable in hot water. Therefore, since according to the phase diagram, the 5YSZ cubic phase must have an yttria content close to 8 mol%, it might be expected that intergranular fracture would also be found in the latter material when loaded in hot water. The present tests with 8YSZ specimens show that this does not happen. No intergranular fracture could be detected, and within the limited test matrix no effect of water on the fracture time was found in 8YSZ. This shows that still another factor besides the presence of water and stress is required for intergranular fracture to occur.

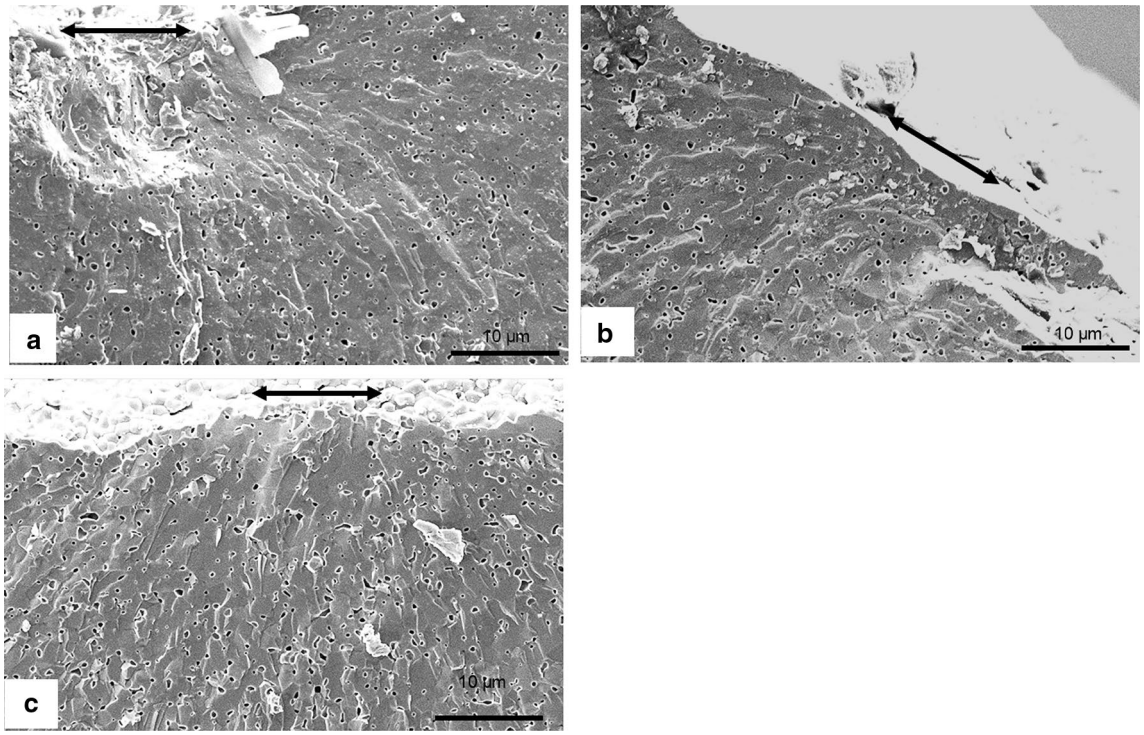


**Fig. 14** Transgranular fractures in 8YSZ. Double arrows indicate crack initiation region **a** broken during proof test in air, **b** broken in autoclave during exposure and **c** broken after exposure in autoclave

Therefore, the present results on 8YSZ were compared with the literature. Specimens made of Tosoh powder were exposed for 2 years at 250 °C to argon containing water *vapour* by Guo and He [16]. These samples showed only transgranular cracking but this does not exclude that testing in *liquid water* might have caused intergranular cracking since water may leach some elements or cause electrochemical processes, phenomena which do not occur in vapour.

A similar set of tests was performed by Siebert-Timmer and Bichler [6], using another, not specified 8YSZ powder type which was spark sintered and hot pressed for 7 min at 1400 °C. The samples were exposed to supercritical water at 400 °C for about 10 h. This material, with a grain size of 20 µm, showed fully *intergranular* fracture, even in the as-sintered condition. After supercritical water exposure, considerably more intergranular cracks could be seen. The intergranular fracture found by Bichler et al. might result from the powder type or from the sintering method which, due to the very short sintering time, may have produced a material with high residual stress. However, the increased intergranular cracking during critical water exposure could be an effect of crack growth in hot water similar to 5YSZ.

From the above, no clear picture appears which would explain intergranular cracking at cubic grain boundaries in hot water. The presence of a thin glassy layer was considered as well. However, in the present study, OM and SEM showed a glassy phase only at a limited number of grain boundaries. Within the detection limits of SEM, most grain boundaries were seen to be free of a continuous second phase. This agrees with high-resolution TEM examinations, described in the literature, which show the absence of amorphous phases at grain boundaries in several ceramics [18, 19, 26, 27]. Therefore, a glassy phase can probably be excluded as the cause of intergranular fracture in the 5YSZ. However, this does not exclude its presence at a nanometre scale. Alternatively, aluminium, silicon or other impurities might be segregated (or depleted) *as solute* at the grain boundaries. However, in the present study it was not foreseen to make a detailed investigation of these possibilities.

## 6 Conclusions

A study was made of the effect of an externally applied bending stress on the cracking mode of industrially produced 5 mol% yttria-zirconia (5YSZ) in water at 300 °C.

In the absence of stress, the selected batch shows no degradation which might inhibit its use for a pH sensor.

Application of an external stress causes initially slow growth of an intergranular crack, followed by catastrophic

transgranular rupture. This proves that the presence of stress is a prerequisite for degradation as set forward at the beginning of this study. This also explains previous results which related the sensitivity to degradation to the amount of intergranular tetragonal precipitates.

The cubic 8YSZ, used in this study for comparison, shows no intergranular degradation. However, literature data show that intergranular fracture in some types of 8YSZ *may* occur. As discussed in Sect. 5, a possible cause for *intergranular* fracture in the presence of stress and water might be the presence of minor elements (Al, Si or other) at the grain boundaries.

The practical problem of degradation is likely to be solved by a reduction in the amount of intergranular tetragonal precipitates to avoid harmful transformation stresses.

## Compliance with ethical standards

**Conflict of interest** On behalf of all authors, the corresponding author states that there is no conflict of interest.

## References


1. Atkinson A, Selçuk A (2000) Mechanical behavior of ceramic oxygen ion-conducting membranes. Solid State Ion 134:59–66
2. Tietz F, Sebold D, Brisse A, Schefold J (2013) Degradation phenomena in a solid oxide electrolysis cell after 9000 h of operation. J Power Sources 223:129–135
3. Radford KC, Bratton RJ (1979) Zirconia electrolyte cells. J Mater Sci 14:59–65
4. Schroer C et al (2011) Design and testing of electrochemical oxygen sensors for service in liquid lead alloys. J Nucl Mater 415:338–347
5. Mariën A, Lim J, Rosseel K, Vandermeulen W, Van den Bosch J (2012) Solid electrolytes for use in lead–bismuth eutectic cooled nuclear reactors. J Nucl Mater 427:39–45
6. Siebert-Timmer A, Bichler L (2015) Degradation of spark plasma sintered yttria stabilized zirconia and $CeO_2$–YSZ ceramics in supercritical water. Int J Appl Ceram Technol 12(6):1103–1111
7. Bosch R-W, Wéber M, Vandermeulen W (2009) Development and testing of an in-core YSZ high-temperature reference electrode. Power Plant Chem 11(4):198–205
8. Vandermeulen W, Bosch R-W (2008) Degradation of 5 mol% $Y_2O_3$–$ZrO_2$ used for the YSZ membrane electrode in high temperature water (300°C). In: Proceedings of international conference on water chemistry of nuclear reactor systems, Berlin, Germany
9. Vandermeulen W, Bosch R-W, Leenaers A, Van Renterghem W, Snijkers F (2010) Degradation of 5 mol% yttria–zirconia by intergranular cracking in water at 300°C. J Mater Sci 45:5502–5511
10. Scott HG (1975) Phase relationships in the zirconia-yttria system. J Mater Sci 10:1527–1535
11. Nakajima K, Kobayashi K, Murata Y (1984) Phase stability of Y-PSZ in aqueous solutions. In: Claussen N, Rühle M, Heuer AH (eds) Science and technology of zirconia II. Advances in ceramics, vol 12. American Ceramic Society, Columbus
12. Sato T, Shimada M (1985) Transformation of yttria doped tetragonal $ZrO_2$ polycrystals by annealing in water. J Am Ceram Soc 68(6):356–359
13. Guo X (1999) On the degradation of zirconia ceramics during low-temperature annealing in water or water vapor. J Phys Chem Solids 60:539–546
14. Chevalier J, Cales B, Drouin JM (1999) Low temperature aging of 3Y-TZP ceramics. J Am Ceram Soc 82(8):2150–2154
15. Hirano M (1992) Inhibition of low temperature degradation of tetragonal zirconia ceramics—a review. Br Ceram Trans J 91:139–147
16. Guo X, He J (2003) Hydrothermal degradation of cubic zirconia. Acta Mater 51:5123–5130
17. Schubert H, Claussen N, Rühle M (1984) Surface stabilization of Y-TZP. Proc Br Ceram Soc 34:157–160
18. Zhang TS, Ma J, Chen YZ, Luo LH, Kong LB, Chan SH (2006) Different conduction behaviors of grain boundaries in $SiO_2$ containing 8YSZ and CGO20 electrolytes. Solid State Ion 177:1227–1235
19. Matsui K, Yoshida H, Ikuhara Y (2008) Grain boundary structure and microstructure development mechanism in 2–8 mol% yttria-stabilized zirconia polycrystals. Acta Mater 56:1315–1325
20. Becher PF (1986) Subcritical crack growth in partially stabilized $ZrO_2$. J Mater Sci 21:297–300
21. Bansal GK, Heuer AH (1975) Precipitation in partially stabilized zirconia. J Am Ceram Soc 58:235–238
22. Porter DL, Heuer AH (1977) Mechanisms of toughening partially stabilized zirconia. J Am Ceram Soc 60(3–4):183–184
23. Hughan RR, Hannink RHJ (1986) Precipitation during controlled cooling of magnesia partially stabilized zirconia. J Am Ceram Soc 69(7):556–563
24. Quinn GD (2007) Fractography of ceramics and glasses. Special publication 960-16. National Institute of Standards and Technology, Gaithersburg
25. Rooke DP, Cartwright DJ (1976) Compendium of stress intensity factors. The Hillingdon Press, Middlesex, p 86
26. Gremillard L, Epicier T, Chevalier J, Fantozzi G (2005) Effect of cooling rate on the location and chemistry of glassy phases in silica doped 3Y-TZP. J Eur Ceram Soc 25:875–882
27. Ross IM, Rainforth WM, McComb DW, Scott AJ, Brydson R (2001) The role of trace additions of alumina to yttria tetragonal zirconia polycrystals. Scr Mater 45:653–660